Hindawi
International Journal of Aerospace Engineering
Volume 2021, Article ID 8872812, 10 pages
https://doi.org/10.1155/2021/8872812

Research Article

Effects of Heat Addition on Wave Drag Reduction of a Spiked Blunt Body

Hongyu Wang, Yanguang Yang, Langquan Li, Gang Wang, and Qinghu Zhang

China Aerodynamics Research and Development Center, 621000 Sichuan Province, China

Correspondence should be addressed to Yanguang Yang; yangyanguang@cardc.cn

Received 5 April 2020; Revised 15 October 2020; Accepted 21 December 2020; Published 16 January 2021

Academic Editor: Dakun Sun

Drag reduction technology plays a significant role in extending the flight range for a high-speed vehicle. A wave drag reduction strategy via heat addition to a blunt body with a spike was proposed and numerically validated. The heat addition is simulated with continuous heating in a confined area upstream of the blunt body. The effects of heat addition on drag reduction in three flow conditions ($M = 3.98, 5, 6$) were compared, and the influence of power density q_h ($q_1 = 2.0 \times 10^8$ W/m^3, $q_2 = 5.0 \times 10^8$ W/m^3, and $q_3 = 1.0 \times 10^9$ W/m^3) of heating was evaluated. Results show that the heat addition has a positive way to reduce the drag of the body with a spike alone, and more satisfactory drag reduction effectiveness can be achieved at a higher Mach number. The drag reduction coefficient increases with q_h in the same flow condition, with a maximum of 38.9% ($M = 6$) as $q_3 = 1.0 \times 10^9$ W/m^3. The wave drag reduction principle was discussed by a transient calculation, which indicates that the separation region has entrainment of the heated air and expanded with its sonic line away from the blunt cone, which results in an alleviation of the pressure load caused by shock/shock interaction.

1. Introduction

The wave drag on a vehicle due to the increase in entropy across the shock wave surrounding a blunt body in high-speed flight is a serious consideration in its aerodynamic design. The huge wave drag not only reduces the speed range and payload but also increases fuel consumption. One way to alleviate the wave drag is to alter the flow in front of the body [1], and the structural spike at the nose of a blunt body is well known, which can reduce the wave drag significantly [2–4]. Therefore, a growing number of studies have been granted on various configurations of these devices to optimize their performance in drag reduction [5–7].

The strong bow shock wave off the wall of the blunt body can be effectively pushed upstream by the spike. A typical structure formed by a blunt body with a spike is shown in Figure 1. A conical shock is generated by the spike, which can alter the flow condition upstream of the blunt body. The spike promotes the flow upstream of the body separated, along with a long shear layer caused by the separation flow, which attaches to the body surface. Hence, a recirculation zone is formed in the flow field near the head of the blunt body. The original bow shock is distorted through interaction with the conical shock and the recirculation zone, which results in a severe reduction of drag imposed on the wall. Research shows that installing a spike on the head of a high-speed vehicle has been proved to be a simple and effective approach to reduce the wave drag.

The effects of spike configuration on their performance in drag reduction in various flow conditions have aroused widespread concern in recent years. Series of experiments have been carried out by Menezes et al. [8], who evaluated the feasibility of using different spike/aerodisk assemblies as retractable drag reduction devices for large-angle blunt cones at a nominal Mach number of 5.75. From their studies, a comprehensive summary of the experimental research shows that forward-facing aerodisks result in a substantial reduction in wave drag, which achieves better effectiveness than spikes without aerodisks for small angles. However, it is also pointed out that at higher angles of attack, the drag increases

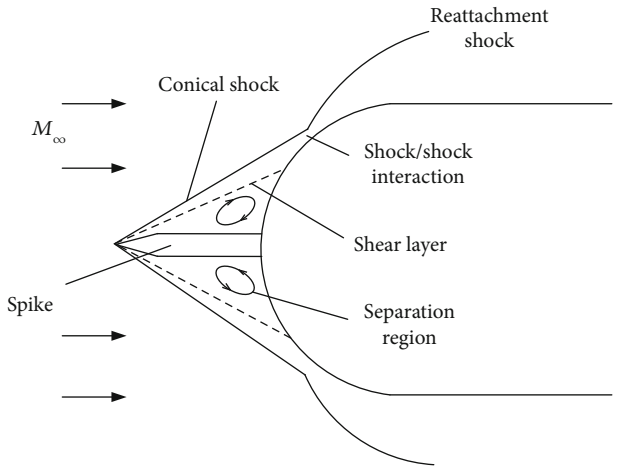

Figure 1: Flow field over a spiked blunt body.

due to the inward shift in the point of impingement of the flow separation shock on the windward side of the cone. Extensive numerical simulations have also been carried out on numerous spiked configurations (different lengths, shapes, and nose configurations). Tahani et al.'s numerical results [9] also demonstrate that the aerodisk is more effective than a spike in drag reduction. The superiority of the aerodisk in reducing the drag was explained by Ahmed and Qin [10], who found that the drag reduction provided by the aerodisk depends on both spike length and aerodisk size. For a specific spike length, there existed an optimum aerodisk size that would produce the minimum drag. A three-dimensional numerical simulation conducted by Kurbatskii and Montanari [11] showed that the spike-aerodisk configuration provides helpful protection to the missile payload in cruise conditions at very low angles of attack. However, at extreme angles of attack, the spike has a detrimental effect by increasing pressure and thermal loads on the missile.

For thermal protection considerations, the opposing jet [12–15], the combinational spike, and the opposing jet concept [16–18] were proposed. In-depth drag reduction mechanism studies on the opposing jet have been widely conducted. Up to now, the combinational concept has become the research hotspot in drag reduction, which combines the merits from the spike in drag reduction and counterflow jet in thermal protection [19]. Experimental investigations on new conceptual methods were reviewed in detail by Wang et al. [20]. In addition, work has also been carried out using plasma or other active energy addition (laser, microwave, etc.) to reduce hypersonic drag and aeroheating loads [21, 22].

Even though the spike has shown its potential in hypersonic drag reduction, there are some problems that remained to be solved. On the one hand, the unsteady nature of the flow due to shock interaction/flow separation may cause fatigue damage, which are subjects of ongoing research [23]. On the other hand, as shown in Figure 1, in some flow conditions, the spike would have a detrimental effect by increasing pressure and thermal loads due to shock/shock interactions near the surface of the blunt body. Therefore, optimal design with an in-depth understanding is still deserved to be done for improving the performance of these devices.

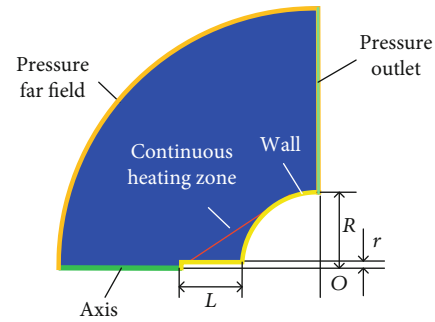

Figure 2: Physical model and boundary conditions in the simulation.

Table 1: Freestream conditions.

M	P_0 (MPa)	T_0 (K)	T_∞ (K)	ρ (kg/m^3)
3.98	1.37	397	95.2	0.339
5.0	0.645	372	62	0.068
6.0	0.83	450	54.9	0.033

The present work is intended as an exploratory study of the possibility of a novel control strategy, a spiked blunt body with heat addition. The purpose of using this strategy goes to alleviate the high-pressure load due to shock/shock interactions to further decrease the wave drag. By using heat addition into the flow, the flow parameters upstream of a blunt body will be changed (such as a decrease of the Mach number). So the structure of a shock wave can be altered so that the pattern of shock/shock interactions will be changed. In the current study, a representative physical model was adopted, and the heat addition is simulated with a continuous heat addition into the flow field. Most of the experiments and simulations related to the heat addition method (laser, arc discharge) generally focused on their upstream effects [24, 25]. In contrast, in this study, the heat addition was considered to be arranged downstream of the shock wave. The effectiveness of the new strategy on drag reduction in various flow conditions was explored by numerical simulation, and the physical interpretation of the effects aroused by this strategy was discussed by carefully studying the evolution of the flow.

2. Physical Model and Numerical Approach

2.1. Physical Model. The physical model in the current study is a blunt body with a cylindrical spike installed at its leading edge, as shown in Figure 2. The radius of the blunt body (R) and the spike (r) is, respectively, 25 mm and 2 mm, and the length (L) of the spike is 20 mm ($L/r = 10$). This configuration has been demonstrated to obtain the best drag reduction effect without a counterflow injection in Huang et al.'s study [26]. The center of the blunt body (O) is configured as the origin of the coordinate system. In supersonic/hypersonic flows, the spike raises a conical shock, which interacts with the bow shock off the blunt body, which makes the bow

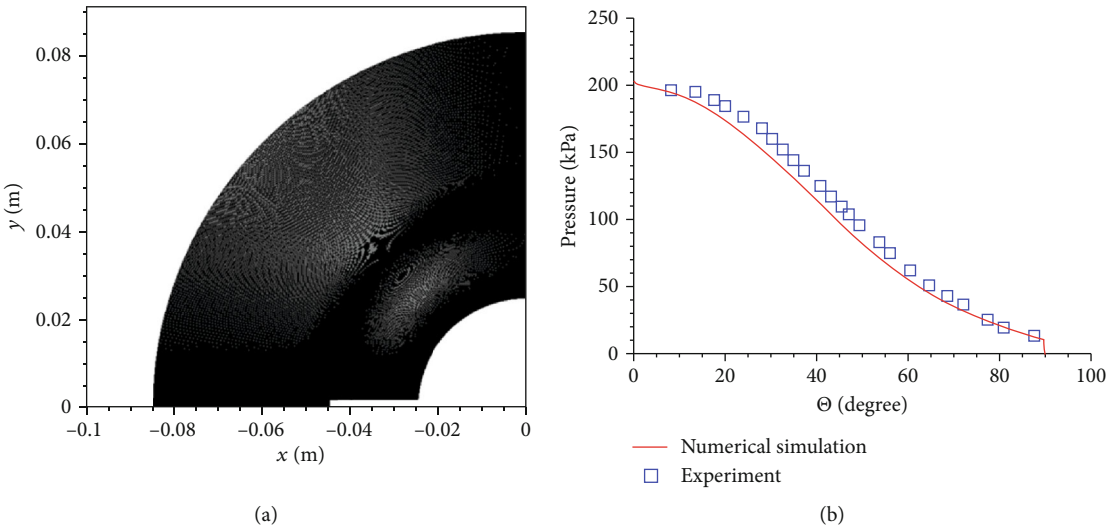

Figure 3: (a) Grid of computation and (b) comparison between the numerical results and the experiment.

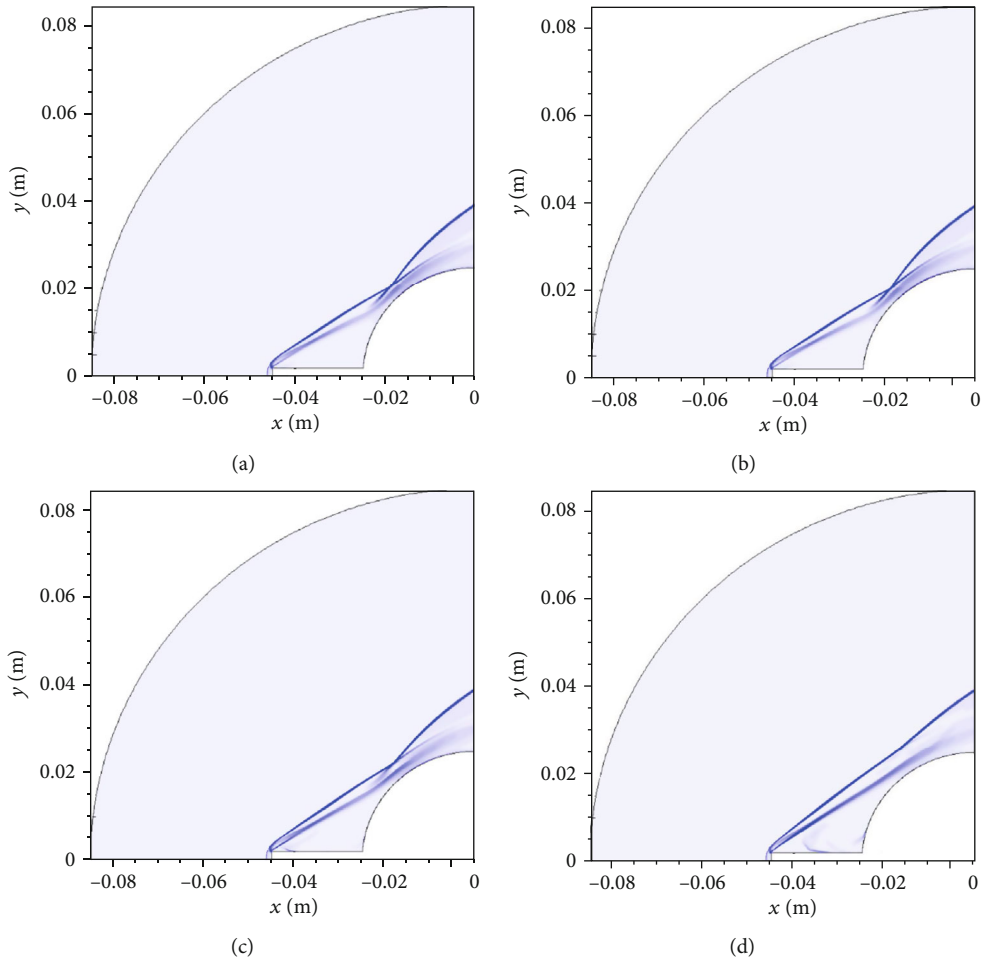

Figure 4: Contours of density gradient magnitude. (a) M5_spike, (b) M5_spike_q1, (c) M5_spike_q2, and (d) M5_spike_q3.

shock move upstream, thus reducing the wave drag. A heating zone near the shear layer is set, which supplies continuous heat addition into the flow field, which can be achieved by a direct-current discharge in practice [27]. The heating zone $S(x, y)$ is confined in an area, as equation (1), a parallelogram one near the shear layer. It is speculated that the heated air will propagate downstream and influence the entire structure of the flow field. The effects of various

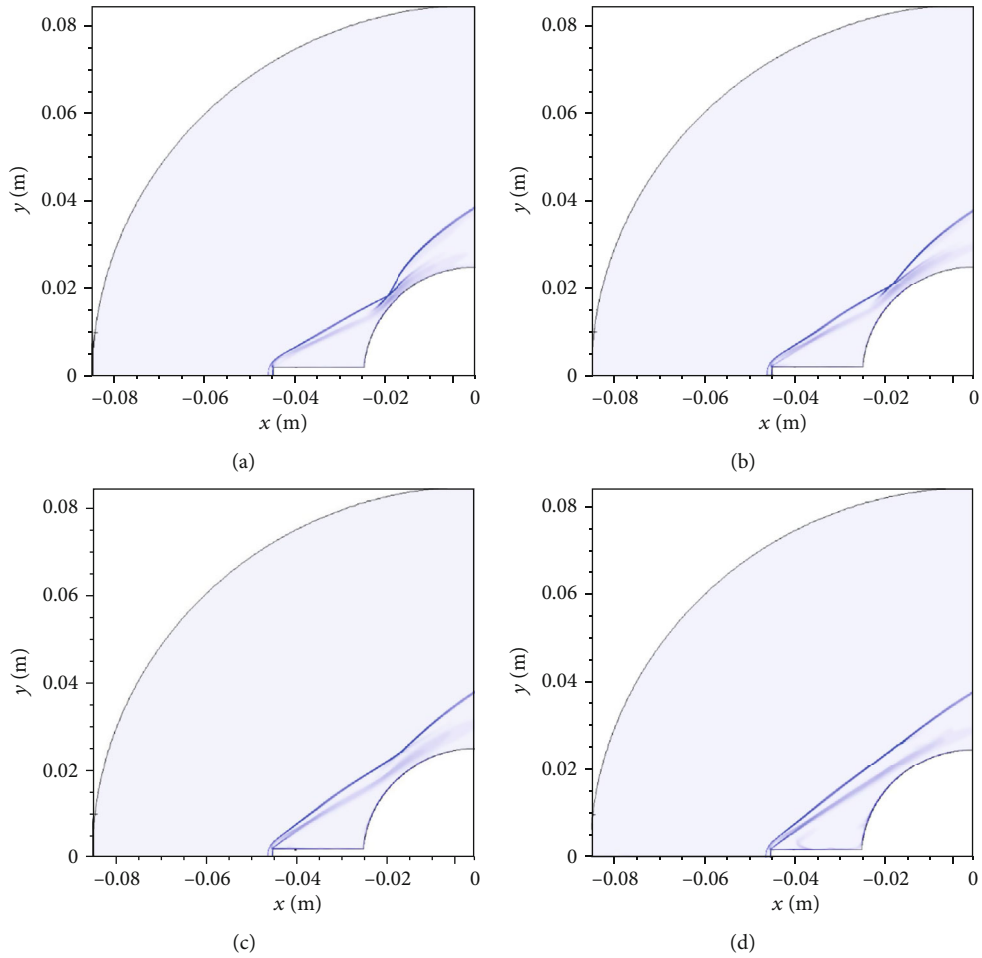

Figure 5: Contours of density gradient magnitude. (a) M6_spike, (b) M6_spike_q1, (c) M6_spike_q2, and (d) M6_spike_q3.

quantities of heat addition on drag reduction were compared.

$$S(x,y)=\begin{cases} -0.045 \le x \le -0.01, \\ 0.65428x + 0.0294 \le y \le 0.65428x + 0.0314. \end{cases} \quad (1)$$

In order to study the effectiveness of the heat addition on drag reduction under various flow conditions, three different freestreams [2, 26, 28] with Mach numbers of, respectively, 3.98, 5.0, and 6.0 were chosen as the inflow conditions in the simulation. The freestream parameters of these conditions are listed in Table 1. Note that the freestream density of the $M = 3.98$ case is one order of magnitude higher than that of the $M = 5.0$ case and the $M = 6.0$ case.

2.2. Numerical Method. A two-dimensional multiblock grid, as shown in Figure 3(a), was generated by utilizing the Gambit software. The first row of mesh cells is set at the height of 0.01 mm away from the wall, which guarantees $y+ <1$, to meet the requirements of the turbulence model, and the grids near wall boundaries were densified to improve the accuracy of the calculation. The inlet flow conditions are completely consistent with the previous studies [26]. The boundary conditions are labeled in Figure 2, where the surface of the blunt body with a spike is set to be the no-slip and isothermal wall with a temperature of $T_w = 295$ K.

Two-dimensional axisymmetric Reynolds-averaged Navier–Stokes equations, coupled with the SST k-ω turbulence model, were solved in the simulation. A source term, defined as a power density q_h, was cooperated into the energy equation to simulate continuous heating in the flow [27, 29]. The Navier-Stokes equations were differentiated by the finite volume method. For solving the compressible high-speed flow field, the density-based solver was used. The second spatially accurate upwind scheme with the advection upstream splitting approach (AUSM) flux vector splitting is used to quicken the convergence speed, and the Courant number remains at 0.5 with suitable underrelaxation factors to ensure computational stability. Fully implicit schemes are inherently stable for linear systems and are currently preferred for viscous compressible flows. The viscosity is calculated with the help of Sutherland's law [2]. The flow is deemed to be axisymmetric; then, only half of the geometry needs to be modeled. The air is assumed to be a thermally and calorically perfect gas, and the mass-weighted mixing law of viscosity is utilized.

Firstly, a stable flow field with a spike was achieved, and then for the simulation with heat addition, a transient

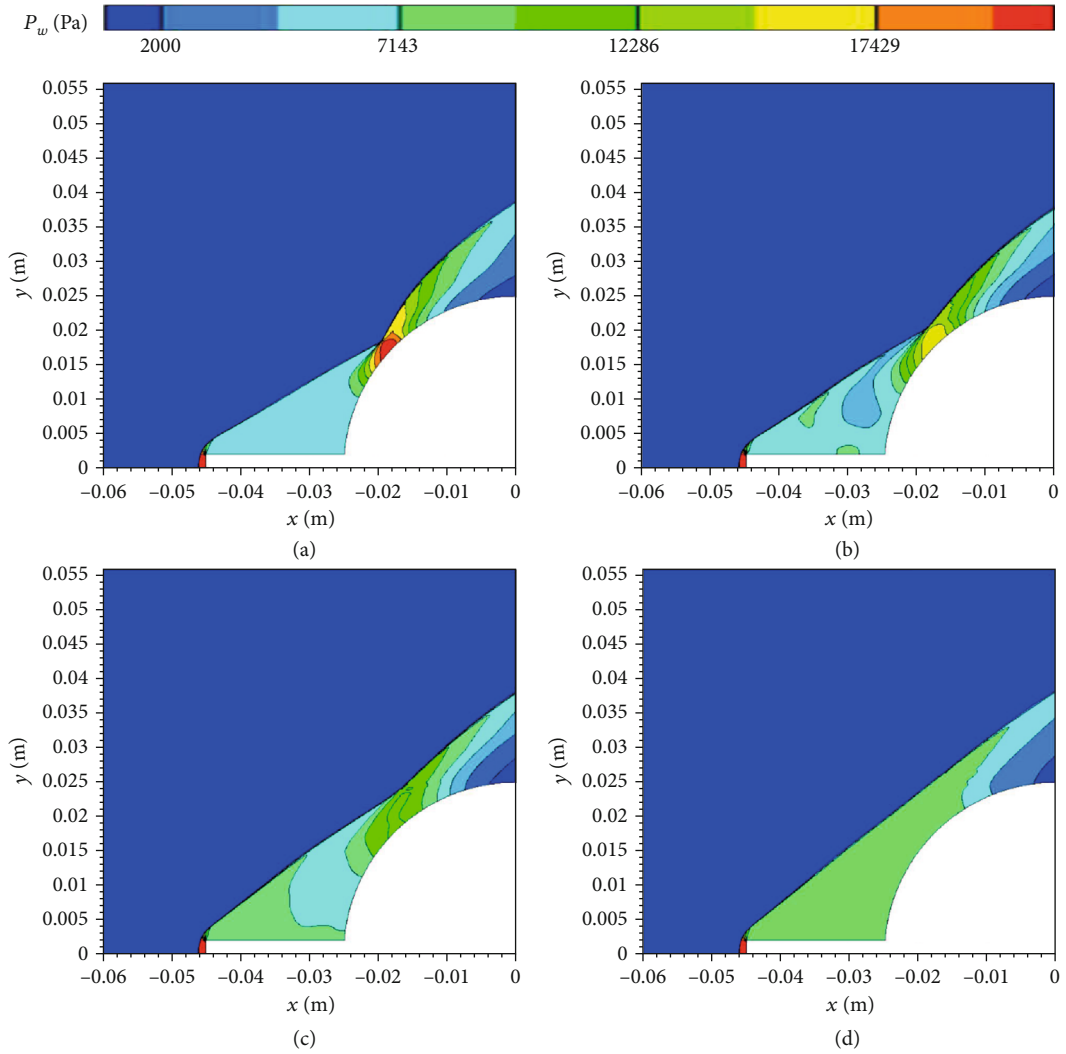

Figure 6: Contours of pressure. (a) M6_spike, (b) M6_spike_q1, (c) M6_spike_q2, and (d) M6_spike_q3.

calculation was adopted. In the transient calculation, the time step was set to be 10^{-8} s, and each step iterated 20 steps, which guaranteed a convergence in each step with time marching. The grid independency analysis based on surface pressure distribution has been carefully carried out in Huang et al.'s study [26]. It has been observed that the numerical results show good agreement with the experimental data, and only a slight impact on the predicted result was found for the coarse, moderate, and refined grid. Therefore, in the current calculation, there are around 320,000 cells for each calculated case, and the comparison between the numerical simulation and the experiment was also made for a blunt body without a spike, as shown in Figure 3(b).

In our simulation [30], the source term (defined as power density q_h) is determined by heating power P and volume of the heating zone V:

$$q = \frac{E}{\tau V} = \frac{P}{V}, \tag{2}$$

where V is a cone-shaped area by $S(x, y)$, rotated about the axis, which is determined by the range of x and y. We chose $q_1 = 2.0 \times 10^8$ W/m^3, $q_2 = 5.0 \times 10^8$ W/m^3, and $q_3 = 1.0 \times 10^9$ W/m^3. According to the value of q_h, the Mach number, and whether the spike is installed on the blunt body, the calculated cases were defined; for example, M5.0_spike_q1 means the Mach number and the power density are 5.0 and 2.0×10^8 W/m^3, respectively, and a spike is installed on the blunt body.

3. Results and Discussion

In this section, the influence of power density on drag reduction of the spiked blunt body was investigated. The drag reduction coefficient was used to evaluate the efficiency of this control strategy, and it was defined as follows:

$$\Delta D = \frac{D - D_0}{D_0} \times 100\%. \tag{3}$$

Herein, ΔD is the drag reduction coefficient. D is the drag force for each case studied, and D_0 is the reference drag force for each Mach number case without spike and heat addition.

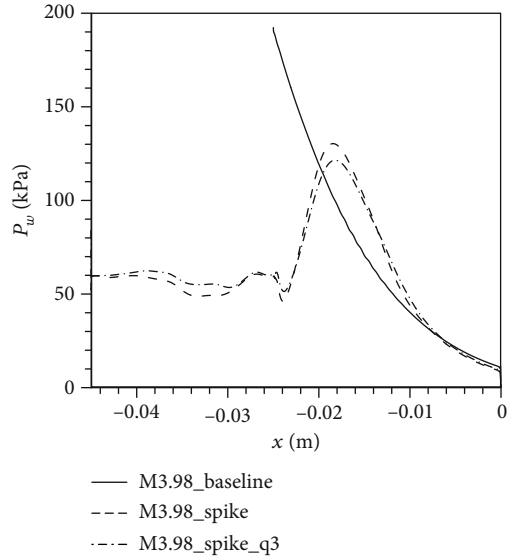

Figure 7: Static pressure distribution comparisons of the M3.98 cases.

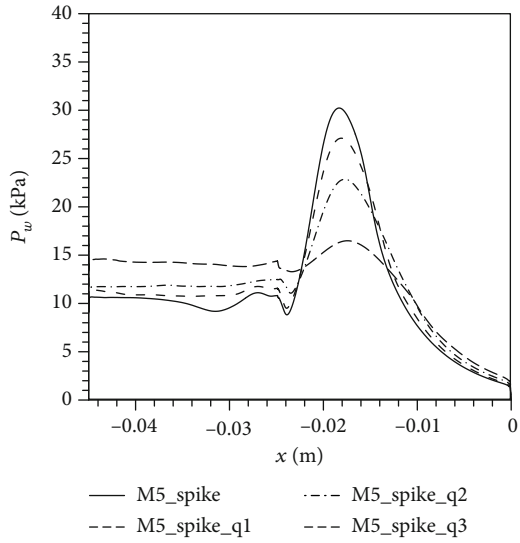

Figure 8: Static pressure distribution comparisons of the M5 cases.

3.1. Influence of Continuous Heating on Wave Drag Reduction. The structure of shock waves induced by a spiked blunt body with and without heat addition was visualized through contours of density gradient magnitude. Without heat addition, as shown in Figures 4(a) and 5(a), it can be seen that the conical shock initiated from the leading edge of the spike and interacted with the bow shock. The shock/shock interaction generally gives rise to a considerable pressure load on the body surface, which attributes to a supersonic jet at the intersection of these shock waves. Meanwhile, shear layers were also depicted underneath the shock waves. With a small quantity of heat addition q_1, as shown in Figures 4(b) and 5(b), the heating zone seems to have little impact on the shock structures. When q_h increases, as shown in Figures 4(c) and 5(c),

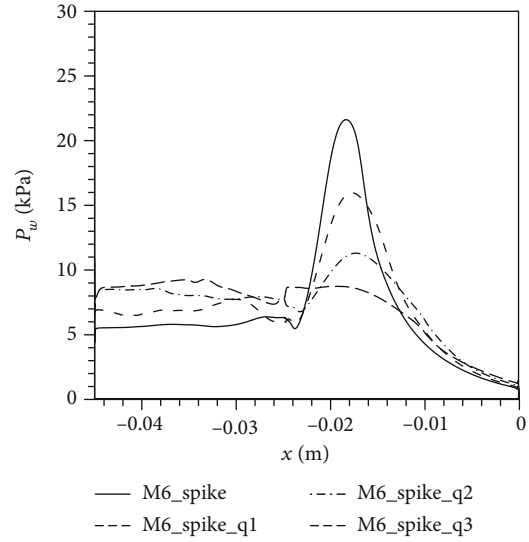

Figure 9: Static pressure distribution comparisons of the M6 cases.

Table 2: Drag force comparison to cases of $M = 3.98$.

Case	D (N)	ΔD (%)
M3.98_baseline	192.91	0
M3.98_spike	158.56	17.78
M3.98_spike_q3	150.36	22.03

Table 3: Drag force comparison to cases of $M = 5$.

Case	D (N)	ΔD (%)
M5_baseline	39.02	0
M5_spike	32.53	16.59
M5_spike_q1	31.36	19.59
M5_spike_q2	29.88	23.38
M5_spike_q3	25.97	33.41

Table 4: Drag force comparison to cases of $M = 6$.

Case	D (N)	ΔD (%)
M6_baseline	24.03	0
M6_spike	20.66	14.02
M6_spike_q1	18.77	21.89
M6_spike_q2	16.09	33.04
M6_spike_q3	14.65	39.03

the interaction pattern of shock waves is altered, with the conical shock moving upward and the intersection point leaving away from the blunt body surface. The shock structures are severely modified if more energy was deposited, as shown in Figures 4(d) and 5(d), which showed that the shock waves did not attach to the blunt body, and the shear layers collapsed into a single one, relatively independent on the shock waves. The shock waves can be pushed away from the blunt body if continuous heating was added into the flow field. Based on the above analysis,

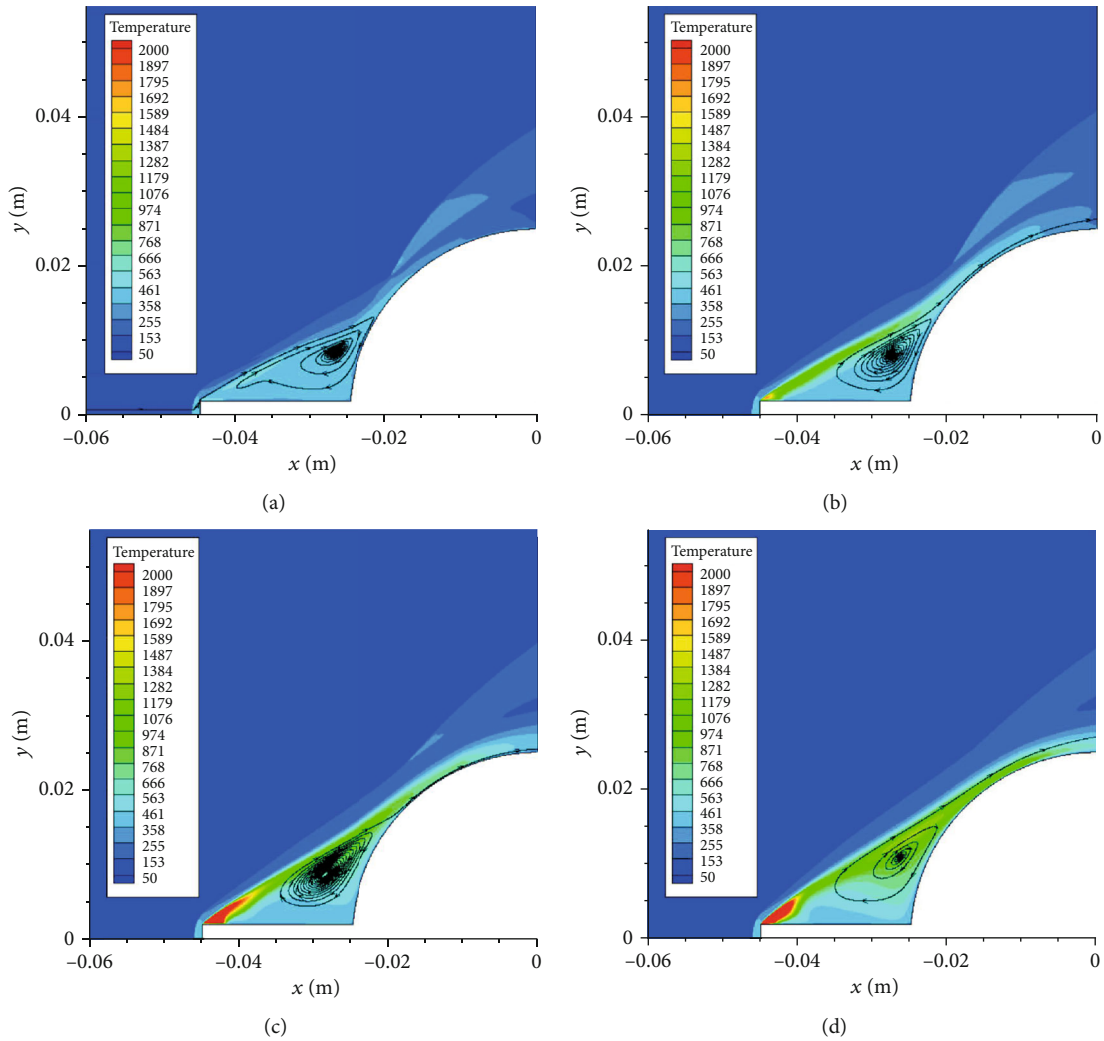

Figure 10: Temperature contours comparisons of the M6 case. (a) $t = 10\,\mu$s, (b) $t = 100\,\mu$s, (c) $t = 200\,\mu$s, and (d) $t = 300\,\mu$s.

it can be speculated that the wave drag can be further reduced due to an alleviation of the pressure load near the surface with heat addition. Note that the shock wave has never been attached on the surface when $q_h = 5.0 \times 10^8$ W/m^3 in the M6 case, as shown in Figure 5(c), in comparison with the M5 case with the same heat addition. Therefore, the comprehensive effect of the heat addition seems to be dominant at a higher Mach number.

Figure 6 shows the pressure contours corresponding to the M6 cases. It can be seen that a severe pressure load existed near the zone of the shock/shock interaction. With heat addition, the shock wave continued to move far away from the surface as q_h increased, as shown in Figures 6(b)–6(d). As a consequence, the pressure load presents a tendency to decrease. Note that the pressure gradient was also decreased downstream of the shock wave due to the heat addition.

Figures 7–9 depict the pressure distribution along the wall of the spiked blunt body. Cases with different power densities in each flow condition were compared. It can be found that the pressure at the front of the body was dramatically decreased by the spike. Through heat addition, the pressure at the zone of shock/shock interaction was further decreased. For cases with a spike in each condition, the peak pressure decreased with an increase of q_h. Note that the pressure at the wall of the spike increases with q_h, which, however, will not contribute to additional axial force. Figure 7 shows that the heat addition seems to have little effect on the drag reduction in $M = 3.98$ cases, which was consistent with the above results. Therefore, the heat addition plays a key role in reducing the regional pressure load in a higher Mach number.

Drag reduction effectiveness aroused by heat addition was evaluated by the drag reduction coefficient ΔD, which is quantitatively listed in Tables 2–4. It showed that for all the conditions, although spike plays a dominant role in wave drag reduction, the maximum coefficient is less than 20% by using a spike. As the Mach number increased, the effect of the spike was decreased, which implied that a spike is less efficient for drag reduction of the blunt body at a higher Mach number. When heat addition was used, the wave drag was

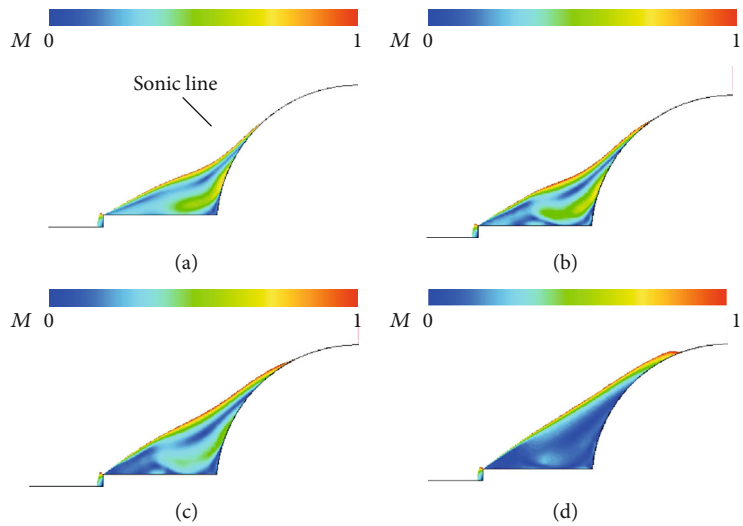

Figure 11: Mach contours in a limited range from 0 to 1 of the M6 case. (a) M6_spike, (b) M6_spike_q1, (c) M6_spike_q2, and (d) M6_spike_q3.

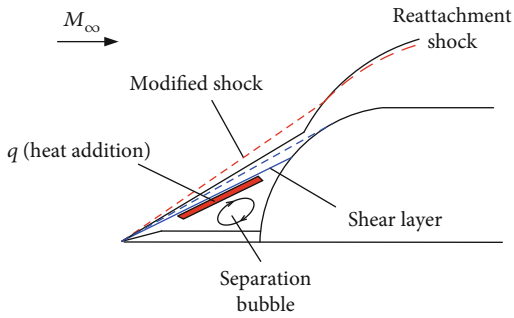

Figure 12: Sketch of a concept for wave drag reduction.

further decreased, and a much more obvious effect was obtained at the higher Mach number. With the same condition, the heat addition brings about a more noticeable effect. The maximum ΔD reaches up to 33.41% for the M5_spike_q3 case and 39.03% for the M6_spike_q3 case. Further, it is also noted that the heat addition has a smaller influence on drag reduction at $M = 3.98$; only 4.25% was increased compared with the case without heat addition.

3.2. Discussion on the Drag Reduction Concept. To give an insight into the control mechanism of the spiked blunt body with heat addition, the transient flow field was further investigated. Figure 10 depicts the evolution of temperature contours of the M6_spike_q3 case. It can be observed that the heated air propagated downstream along the shear layer partially was enrolled in the separation bubble. The separation zone was occupied by high-temperature fluids with heat addition. The heated air tended to be concentrated near the shear layer, where a zone with a much higher temperature was formed. The separation bubble seemed to be inflated because of the enrollment of high-temperature fluids from the heating zone. As a result, the area of subsonic flow was enlarged, with the sonic line moving upward, far away from the blunt body, as shown in Figure 11. Besides, downstream transportation of the heated air increased the local sound velocity, which leads to a decrease in the freestream Mach number, so the intensity of the shock at the wall was reduced to some extent. Therefore, the principle of a further drag reduction is that the shock/shock interaction is alleviated by shifting the conical shock upward through altering the characteristics of the separation bubble.

4. Conclusion

A new control strategy for drag reduction based on a spiked blunt body with heat addition in high-speed flows was proposed and validated by numerical simulation. The numerical method was verified through comparison with the published experimental data. Results show that a further reduction in wave drag can be realized by heat addition into the flow.

The principle of a further drag reduction by using the strategy is depicted through a concept sketch in Figure 12. The physical process can be summarized as follows: the separation zone has entrainment of heated air through the shear layer, where the heated air is concentrated and ultimately propagates downstream along the wall. As a result, the separation zone is expanded with the sonic line lifted away from the blunt body, and the conical shock induced by the spike deviates upward, which alters the position of shock/shock interaction. Hence, the pressure load is alleviated. On the other hand, the Mach number upstream of the interaction zone is decreased, and the shock intensity can be alleviated, which is also a factor in reducing the wave drag.

In the present study, the effect of the control strategy on drag reduction in three flow conditions has been analyzed, and the influence of power density q_h ($q_1 = 2.0 \times 10^8$ W/m^3, $q_2 = 5.0 \times 10^8$ W/m^3, and $q_3 = 1.0 \times 10^9$ W/m^3) of the heating area has been evaluated. Results show that the wave drag of a spiked blunt body can be reduced seriously with heat addition, and more satisfactory effectiveness can be achieved at a higher Mach number. The drag reduction coefficient

increases with q_h in the same flow condition, with the maximum coefficient of 38.9% ($M = 6$), 33.4% ($M = 5$), and 20.5 ($M = 3.98$), respectively, as $q_h = 1.0 \times 10^9$ W/m^3.

Note that although the shock/shock interaction was modified obviously by heat addition, much energy may be consumed, and some ways of getting the most benefit by using the least energy deserve to be studied. On the other hand, during the heat injection, the wall heat transfer is increased, which may bring burdens on a thermal protection system. In further investigation, a wind tunnel experiment will be conducted to validate the control strategy. The heat addition will be realized by direct-current discharge or high-frequency arc plasma energy deposition, and the drag coefficient will be qualitatively measured by an optical fiber balance. Moreover, the control authority of this strategy at a higher angle of attack is worth to be studied.

Data Availability

The data used to support the findings of this study are available from the corresponding author upon request.

Conflicts of Interest

The authors declare that they have no conflicts of interest.

Acknowledgments

This study is supported by the National Key R&D Program of China (Grant No. 2019YFA0405300) and the National Natural Science of China (Grant No. 12002363).

References

[1] B. Meyer and H. F. Nelson, "Hypersonic drag and heat transfer reduction using a forward facing jet," in *9th International Space Planes and Hypersonic Systems and Technologies Conference*, Norfolk, VA, USA, 1999.

[2] K. Mansour and M. Khorsandi, "The drag reduction in spherical spiked blunt body," *Acta Astronautica*, vol. 99, pp. 92–98, 2014.

[3] R. Kalimuthu and E. Rathakrishnan, "Aerospike for drag reduction in hypersonic flow," in *44th AIAA/ASME/SAE/ASEE Joint Propulsion Conference & Exhibit*, Hartford, CT, 2008.

[4] V. Kulkarni, V. Menezes, and K. P. J. Reddy, "Effectiveness of aerospike for drag reduction on a blunt cone in hypersonic flow," *Journal of Spacecraft and Rockets*, vol. 47, no. 3, pp. 542–544, 2010.

[5] M. Barzegar Gerdroodbary and S. M. Hosseinalipour, "Numerical simulation of hypersonic flow over highly blunted cones with spike," *Acta Astronautica*, vol. 67, no. 1-2, pp. 180–193, 2010.

[6] M. Y. M. Ahmed and N. Qin, "Recent advances in the aerothermodynamics of spiked hypersonic vehicles," *Progress in Aerospace Sciences*, vol. 47, no. 6, pp. 425–449, 2011.

[7] M. Kharati-Koopaee and H. Gazor, "Assessment of the aerodisk size on drag reduction and thermal protection of high-bluntness vehicles at hypersonic speeds," *Journal of Aerospace Engineering*, vol. 30, no. 4, article 04017008, 2017.

[8] M. Viren, S. Saravanan, G. Jagadeesh, and K. P. J. Reddy, "Aerodynamic drag reduction using aerospikes for large angle blunt cone flying at hypersonic Mach number," in *22nd AIAA Aerodynamic Measurement Technology and Ground Testing Conference*, St. Louis, Missouri, 2002.

[9] M. Tahani, M. S. Karimi, A. Mahmoudi Motlagh, and S. Mirmahdian, "Numerical investigation of drag and heat reduction in hypersonic spiked blunt bodies," *Heat and Mass Transfer*, vol. 49, no. 10, pp. 1369–1384, 2013.

[10] M. Y. M. Ahmed and N. Qin, "Drag reduction using aerodisks for hypersonic hemispherical bodies," *Journal of Spacecraft and Rockets*, vol. 47, no. 1, pp. 62–80, 2010.

[11] K. A. Kurbatskii and F. Montanari, "Application of pressure-based coupled solver to the problem of hypersonic missiles with aerospikes," in *45th AIAA Aerospace Sciences Meeting and Exhibit*, Reno, Nevada, 2007.

[12] B. Venukumar, G. Jagadeesh, and K. P. J. Reddy, "Counterflow drag reduction by supersonic jet for a blunt body in hypersonic flow," *Physics of Fluids*, vol. 18, no. 11, article 118104, 2006.

[13] V. Kulkarni and K. P. J. Reddy, "Enhancement in counterflow drag reduction by supersonic jet in high enthalpy flows," *Physics of Fluids*, vol. 20, article 016103, 2008.

[14] C. D. Marley and D. W. Riggins, "Numerical study of novel drag reduction techniques for hypersonic blunt bodies," *AIAA Journal*, vol. 49, no. 9, pp. 1871–1882, 2011.

[15] S. Li, W. Huang, J. Lei, and Z. Wang, "Drag and heat reduction mechanism of the porous opposing jet for variable blunt hypersonic vehicles," *International Journal of Heat and Mass Transfer*, vol. 126, pp. 1087–1098, 2018.

[16] W. Huang, L. Yan, J. Liu, L. Jin, and J. Tan, "Drag and heat reduction mechanism in the combinational opposing jet and acoustic cavity concept for hypersonic vehicles," *Aerospace Science and Technology*, vol. 42, pp. 407–414, 2015.

[17] X. Sun, Z. Guo, W. Huang, S. Li, and L. Yan, "Drag and heat reduction mechanism induced by a combinational novel cavity and counterflowing jet concept in hypersonic flows," *Acta Astronautica*, vol. 126, pp. 109–119, 2016.

[18] J. Huang and W. Yao, "Hypersonic drag reduction mechanism of a novel combinational spike and multi-opposing jets aerodynamic configuration," *Acta Astronautica*, vol. 171, pp. 245–256, 2020.

[19] J. Huang, W. Yao, and N. Qin, "Heat reduction mechanism of hypersonic spiked blunt body with installation angle at large angle of attack," *Acta Astronautica*, vol. 164, pp. 268–276, 2019.

[20] Z. Wang, X. Sun, W. Huang, S. Li, and L. Yan, "Experimental investigation on drag and heat flux reduction in supersonic/hypersonic flows: a survey," *Acta Astronautica*, vol. 129, pp. 95–110, 2016.

[21] K. Satheesh and G. Jagadeesh, "Effect of concentrated energy deposition on the aerodynamic drag of a blunt body in hypersonic flow," *Physics of Fluids*, vol. 19, no. 3, article 031701, 2007.

[22] K. Vinayak, G. M. Hegde, G. Jagadeesh, E. Arunan, and K. P. J. Reddy, "Aerodynamic drag reduction by heat addition into the shock layer for a large angle blunt cone in hypersonic flow," *Physics of Fluids*, vol. 20, article 81703, 2008.

[23] Y. Ma, X. Liu, and P. Ou, "Numerical investigation of hypersonic unsteady flow around a spiked blunt-body," *Procedia Engineering*, vol. 126, pp. 163–168, 2015.

[24] T. Taylor, "Drag reduction and control using energetics and electrostatic force-fields for hypersonic applications," in *42nd*

AIAA Aerospace Sciences Meeting and Exhibit, Reno, Nevada, 2004.

[25] E. Erdem, L. Yang, and K. Kontis, "Drag Reduction by Energy Deposition in Hypersonic Flows," in *16th AIAA/DLR/DGLR International Space Planes and Hypersonic Systems and Technologies conference*, Bremen, Germany, 2009.

[26] W. Huang, J. Liu, and Z. Xia, "Drag reduction mechanism induced by a combinational opposing jet and spike concept in supersonic flows," *Acta Astronautica*, vol. 115, pp. 24–31, 2015.

[27] H. Yan, F. Liu, and J. Xu, "Oblique shock control by surface arc discharge plasma," in *8th AIAA Flow Control Conference*, Washington DC, 2016.

[28] E. Erdem, K. Kontis, and L. Yang, "Steady heat addition at Mach 5 for drag reduction," *Shock Waves*, vol. 23, pp. 285–298, 2013.

[29] F. Falempin, A. A. Firsov, D. A. Yarantsev, M. A. Goldfeld, K. Timofeev, and S. B. Leonov, "Plasma control of shock wave configuration in off-design mode of $M = 2$ inlet," *Experiments in Fluids*, vol. 56, no. 3, article 54, 2015.

[30] H. Wang, J. Li, D. Jin, H. Dai, T. Gan, and Y. Wu, "Effect of a transverse plasma jet on a shock wave induced by a ramp," *Chinese Journal of Aeronautics*, vol. 30, no. 6, pp. 1854–1865, 2017.